J Radioanal Nucl Chem (2013) 295:545–552
DOI 10.1007/s10967-012-1883-y

Synthesis and evaluation of a series of ^{99m}Tc-labelled zoledronic acid derivatives as potential bone seeking agents

Ling Qiu · Wen Cheng · Jianguo Lin · Liping Chen · Jun Yao · Wenwen Pu · Shineng Luo

Received: 11 April 2012 / Published online: 19 June 2012

Abstract Developing novel superior bone-seeking radiopharmaceuticals for the detection of malignant bone lesions could further improve the diagnostic value of routine bone scanning. A series of radiolabeled diphosphonates (^{99m}Tc-EIPrDP, ^{99m}Tc-EIBDP and ^{99m}Tc-EIPeDP) have been designed and synthesized successfully in high chemical yields and radiochemical purity. The in vitro and in vivo biological properties were systematically investigated and compared. The biodistribution in mice shows that ^{99m}Tc-EIPrDP has higher bone uptake (13.3 ± 1.23) than those of ^{99m}Tc-EIBDP and ^{99m}Tc-EIPeDP (11.7 ± 0.28 and 8.69 ± 0.04 %ID/g) at 1–2 h post injection. It also has the highest uptake ratio of bone to muscle, spleen and heart, respectively, and faster blood clearance in early times. The present study indicates that ^{99m}Tc-EIPrDP holds great promise as a bone imaging agent.

Keywords Zoledronic acid derivatives · ^{99m}Tc-labelled diphosphonates · Stability · Biodistribution · Bone imaging agent

Introduction

Bone metastasis occurs in almost all cancers, most frequently with prostate, lung, and breast cancers. Nearly 80 % of patients with advanced breast or prostate cancer would develop bone metastasis [1, 2]. These malignant tumor metastases have strong impact on the quality of living for those patients. Severe complications include bone pain, pathologic fracture, hypercalcemia, and spinal cord compression [3]. To detect the bone metastasis at early stage, novel bone imaging agents with high bone affinity are needed to improve the diagnostic accuracy of routine bone scanning [4].

Several ^{99m}Tc-labeled phosphonates have been developed for skeletal imaging, including pyrophosphates [5], polyphosphates [6, 7], and diphosphonates (DPs) [8, 9]. For example, the conjugates between methylenediphosphonate (^{99m}Tc-MDP) and hydroxy-methylenediphosphonate (^{99m}Tc-HMDP) and technetium-99m have been widely used both experimentally and clinically for detection of skeletal metastases and other focal bone lesions [8, 10, 11]. Technetium-99m has excellent physical characteristics ($t_{1/2} = 6.02$ h, $E_\gamma = 142$ keV) and can be easily available from a generator. It has become the most important nuclide for organ imaging in nuclear medicine. Phosphonate derivatives are good targeting ligands for technetium-99m conjugates to be used as bone imaging agents [8], since Fleisch [12] described that phosphonates had high affinity for bone mineral.

Diphosphonates are one class of important clinical drugs for bone disease [13] and are used in the therapy of early cancer treatment to prevent adverse effects of therapies on the bone health [14]. A number of DPs are commercially available, such as clodronate, etidronate, pamidronate, alendronate, ibandronate, tiludronate, incadronate, risedronate, and zoledronate (ZL). However, for these ^{99m}Tc-DPs, an interval of 2–6 h is needed between injection and bone imaging [15]. Shorting this interval would lessen the burden on patients in terms of examination time. To enable imaging at earlier time

L. Qiu · W. Cheng · J. Lin (✉) · L. Chen · J. Yao · W. Pu · S. Luo (✉)
Key Laboratory of Nuclear Medicine, Ministry of Health, Jiangsu Key Laboratory of Molecular Nuclear Medicine, Jiangsu Institute of Nuclear Medicine, Wuxi 214063, China
e-mail: jglin@yahoo.cn

S. Luo
e-mail: shineng914@yahoo.com.cn

after injection, a radiopharmaceutical with higher affinity for bone, larger ratio of bone-to-soft tissue uptake, and more rapid clearance from blood is required [16].

The structure of the tether attached to diphosphates in DPs determines their biological activities. When the carbon chain of the tether increases, the binding affinity for bone increases significantly. For example, from pamidronate to alendronate where the carbon chain increases from 1 to 2, the binding affinity increased 10 times [17]. The dialkylation of the nitrogen with methyl and pentyl groups in pamidronate generated ibandronate. The potency of the latter was 50 times of the former [18]. ZL is the most potent third-generation DPs, and the tether has an imidazole ring [19]. We had evaluated a series of derivatives of ZL with different alkyl substituents in the imidazole ring and different number of methylene linker between the imidazole ring and geminal diphosphonate groups in our previous publications [20–27]. We found significant improvement on bone absorption and clearance from blood and soft tissues.

In this paper, we report our evaluation on a new series of ZL derivatives (Scheme 1). We examined their in vitro stability and in vivo biodistributions in mice.

Experimental

Reagents, instruments and animals

All analytical chemical reagents were purchased from commercial sources and used without further purification. $Na^{99m}TcO_4$ and human serum were supplied by affiliated Jiangyuan Hospital of Jiangsu Institute of Nuclear Medicine. Melting points were measured on Yanaco MP-500 melting point apparatus (Shimadzu, Japan). Elemental analysis was carried out using an Elementar Vario EL III analyzer. Electron spray ion (ESI) mass spectra were determined using a Waters Platform ZMD4000 LC/MS (Waters, USA). Proton nuclear magnetic resonance (^{1}H NMR) spectra were obtained on a Bruker DRX-500 spectrometer (Bruker, Germany), and the chemical shift values were referenced to the internal tetramethylsilane (TMS). The Xinhua chromatography paper (Shanghai, China) was used for Mini-Scan and Flow-count thin paper chromatography (TLC) (BIO-SCAN, USA). A Packard-multi-prias γ counter (Perkins Elmer, USA) were used for radioactive counting. The high performance liquid chromatography (HPLC) system was equipped with a Waters 1525 binary HPLC pump, a Waters 2487 dual wavelength absorbance detector, and a Perkin Elmer Radiomatic 610TR radioactivity detector, which were operated by Breeze and proFSA software. A reverse phase C_{18} (RP-C_{18}) column (4.6 × 250 mm; 10 μm particle size) was used for HPLC analysis (Elite Analytical Instrument Company, Dalian, China).

Institute of Cancer Research (ICR) mice (weighing 18–24 g) were supplied by Shanghai SLAC Laboratory Animal Co. Ltd. (Shanghai, China). The animal experiment in this study was approved by the Animal Care and Ethics Committee of Jiangsu Institute of Nuclear Medicine.

Syntheses of EIPrDP, EIBDP, and EIPeDP

These diphosphonic acids were synthesized according to the procedure outlined in Scheme 1 [26–29].

Syntheses of compounds **2**

Compound **1** (0.1 mol) was dissolved in CH_2Cl_2 (75 mL), followed by adding KOH (8.4 g, 0.15 mol), K_2CO_3 (13.8 g, 0.0835 mol) and N(*n*-Bu)$_4$Br (0.7 g, 0.002 mol). The solution was treated with homolog of ethyl bromoacetate (0.1 mol) and heated to reflux for 7 h. To remove the inorganic salt, the solution was filtered and the filtrate was washed with brine solution. After drying, the organic phase was evaporated to give the ester of compound **2**, which was used without further purification. HCl (1.2 mol/L, 100 mL)

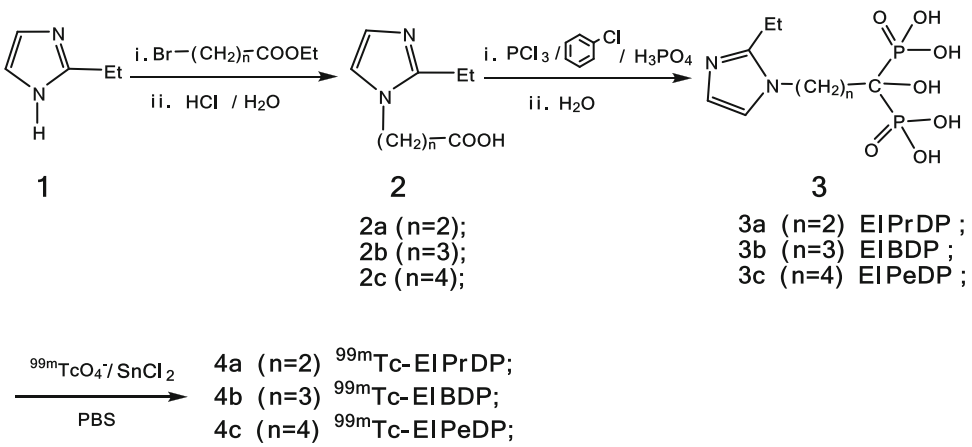

Scheme 1 Syntheses of ^{99m}Tc-EIPrDP, ^{99m}Tc-EIBDP, and ^{99m}Tc-EIPeDP

was added to the ester of compound **2** and the mixture was refluxed for 8 h. The solution was concentrated and the residue was recrystallized from isopropanol to give the product **2**.

*3-(2-Ethyl-1H-imidazol-1-yl) propanoic acid (**2a**)*: Yield, 58 %. mp 105–107 °C; ESI–MS, m/z (%): 167 (100, $[M–H]^+$).

*4-(2-Ethyl-1H-imidazol-1-yl) butanoic acid (**2b**)*: Yield, 36 %. mp 145–147 °C; ESI–MS, m/z (%): 181(100, $[M–H]^+$).

*5-(2-Ethyl-1H-imidazol-1-yl) pentanoic acid (**2c**)*: Yield, 60 %; ESI–MS, m/z (%): 195(100, $[M–H]^+$).

Syntheses of compounds **3**

Compound **2** (20 mmol) was dissolved in chlorobenzene (25 mL) and heated to 120 °C for 30 min, then phosphoric acid (85 %, 4.2 mL) was added. Phosphorus trichloride (7.6 mL) was added dropwise, and the reaction mixture was kept at 120 °C for 4 h. The chlorobenzene was decanted. The yellow residue was redissolved in HCl (9 mol/L, 20 mL) and heated to reflux for 5 h. Charcoal was added before filtration to decolor the solution. After filtration, the solvent was removed. Finally, the crude product was recrystallized from ethanol to give the white crystalline product **3**.

*1-Hydroxy-3-(2-ethyl-1H-imidazol-1-yl)propane-1,1-diyldiphosphonic acid (**3a**)*: Yield, 43 %. mp 185–188 °C; ^{1}H NMR (400 MHz, D_2O): δ7.348 (d, $J = 1.6$ Hz, 1H, CH-ring), 7.235 (d, $J = 1.6$ Hz, 1H, CH-ring), 4.395–4.354 (m, 2H, N–CH_2), 2. 956 (dd, $J = 7.6$ Hz, 2H, ring-CH_2), 2.429–2.319 (m, 2H, HO–C–CH_2), 1.305–1.267 (t, $J = 7.6$ Hz, 3H, –CH_3); ESI–MS, m/z (%): 313(100, $[M–H]^+$). Anal. calcd for $C_8H_{16}N_2O_7P_2$ (%): C, 30.58; H, 5.13; N, 8.92; Found (%): C, 30.62; H, 5.23; N, 9.11.

*1-Hydroxy-4-(2-ethyl-1H-imidazol-1-yl)butane-1,1-diyldiphosphonic acid (**3b**)*: Yield, 31 %. mp 200–203 °C; ^{1}H NMR (400 MHz, D_2O): δ7.362 (d, $J = 1.6$ Hz, 1H, CH-ring), 7.262 (d, $J = 1.6$ Hz, 1H, CH-ring), 4.111 (t, $J = 7.2$ Hz, 2H, N–CH_2), 2.990–2.933 (dd, $J = 7.6$ Hz, 2H, ring-CH_2), 2.149–2.091 (m, 2H, HO–C–CH_2), 1.954–1.915 (m, 2H, CH_2–CH_2–CH_2), 1.309–1.271(t, $J = 7.6$ Hz, 3H,–CH_3); ESI–MS, m/z (%): 327(100, $[M–H]^+$). Anal. calcd for $C_9H_{18}N_2O_7P_2$ (%): C, 32.94; H, 5.53; N, 8.54; Found (%): C, 33.02; H, 5.64; N, 8.61.

*1-Hydroxy-5-(2-ethyl-1H-imidazol-1-yl)pentane-1,1-diyldiphosphonic acid (**3c**)*: Yield, 29 %. mp 75–78 °C; ^{1}H NMR (400 MHz, D_2O): δ7.324 (d, $J = 1.6$ Hz, 1H, CH-ring), 7.251 (d, $J = 1.6$ Hz, 1H, CH-ring), 4.084 (t, $J = 7.2$ Hz,2H, N–CH_2), 3.610–3.557 (dd, $J = 7.2$ Hz, 2H, ring-CH_2), 2.963–2.906 (q, 2H, HO–C–CH_2), 1.849–1.776 (m, 2H, CH_2–CH_2–COH), 1.306–1.269 (m, 2H, ring-CH_2CH_2), 1.129–1.094(t, $J = 6.8$ Hz, 3H, –CH_3); ESI–MS, m/z (%): 342(100, $[M–H]^+$). Anal. calcd for $C_{10}H_{20}N_2O_7P_2$ (%): C, 35.10; H, 5.89; N, 8.19; Found (%): C,35.08; H, 6.02; N, 8.29.

Radiolabeling

To a 10 mL vial, 100 μL **3a–3c** aqueous solution (0.25 g DPs dissolved in 5.0 mL 0.2 M sodium hydroxide solution), 100 μL freshly prepared solution of stannous chloride dihydrate (10 mg $SnCl_2{\cdot}2H_2O$ dissolved in 10.0 mL 0.5 M HCl solution), and 74.0 MBq freshly eluted $Na^{99m}TcO_4$ were added. After the pH value of the reaction system was adjusted to 6.0 by adding 0.2 M phosphate buffer solution (PBS) and diluted to 2 mL, the reaction mixture was kept at 70 °C for 30 min.

Quality control

The radiolabeling yield (RLY) of **4a–4c** was determined by TLC. Strips of Xinhua No.1 paper chromatography of 13 cm long and 0.5 cm wide were marked at 1.5 cm from the bottom and was lined into sections 1 cm each, up to 10 cm. About 3 μL ^{99m}Tc-EIPrDP, ^{99m}Tc-EIBDP and ^{99m}Tc-EIPeDP solution was applied with a syringe at 1.5 cm from the bottom of each paper strip, and then these strips were developed in distilled water and acetone. After complete development, the strips were dried and assayed by Mini-Scan TLC. The RLY of **4a–4c** were determined as follows: % RLY = 100 % − % free $^{99m}TcO_4$ − % ^{99m}Tc-colloidal.

The radiochemical purity (RCP) of **4a–4c** was determined by HPLC. The sample was filtered through a 0.22 μm Millipore filter carefully and 10 μL solution was injected into the HPLC column. The column was eluted with isocratic solvents of 70 % water and 30 % acetonitrile, and the flow rate was 1.0 mL/min. Radio-analysis of the labeled compound was performed using a Cd (Te) detector.

In vitro stability

The in vitro stability of ^{99m}Tc-EIPrDP, ^{99m}Tc-EIBDP and ^{99m}Tc-EIPeDP were studied in PBS (pH = 7.4), fetal bovine serum (FBS), or human serum (HS) for 1–6 h. Briefly, 200 μL (3.7 MBq) of ^{99m}Tc-EIPrDP, ^{99m}Tc-EIBDP and ^{99m}Tc-EIPeDP were pipetted into 200 μL of PBS, FBS, or HS, respectively. After incubation at 37 °C for 1–6 h, an aliquot of PBS solution were taken directly and radioactivity was analyzed with TLC. For the solution of FBS and HS, the aliquot were added to 100 μL of 50 % trifluoroacetic acid (TFA). After centrifugation, the upper solution was taken for TLC analysis.

Determination of octanol–water partition coefficient (Log *P*)

The octanol–water partition coefficient was determined for **4a–4c** at pH = 7.4 by measuring the distribution of the radiolabeled compounds in *n*-octanol and PBS, respectively. A 100 μL sample of **4a–4c** was diluted with 900 μL PBS. Then, it was mixed with 1 mL *n*-octanol and vortexed for 5 min. The mixture was further centrifuged at 4,000 rpm for 5 min to ensure complete separation of layers. 100 μL aliquots of organic and aqueous phases were collected with pipettor and the radioactivity was measured with a γ counter, respectively. The octanol–water partition coefficient (log *P*) was calculated using the formula log *P* = log (octanol CPM/PBS CPM) [30]. The reported value is the average obtained from three independent experiments.

Plasma protein binding assay

4a–4c (100 μL, 37 KBq) were mixed with the human plasma (100 μL) in the centrifuge tube. After the mixture was incubated at 37 °C for 2 h, the plasma protein was precipitated by adding 1 mL trichloroacetic acid (250 g/L) to the mixture. The supernatant and precipitate were separated by centrifugation at 3,000 rpm for 5 min. The radioactivities of both phases were measured separately. The above experimental procedure was repeated three times. The percentage of protein binding was determined by the following equation: Plasma protein binding % = (Precipitate CPM)/[Precipitate CPM + Plasma CPM]) × 100 %.

Kinetics of blood clearance

For pharmacokinetic study, **4a–4c** (7.4 MBq, 0.2 mL aqueous solution) was administered to the mice via intravenous injection through the tail vein. A series of blood samples (20 μL) were collected in the microcap tubes by nicking the tail with a needle at 2, 5, 10, 15, 30, 60, 120, 180, and 240 min after injecting **4a–4c**. The radioactivity of the blood samples was counted and expressed as %ID/g. Pharmacokinetic parameters were analyzed by the 3P97 software (Practical Pharmacokinetic Program from China's pharmacological to learn mathematics professional committee), and the radioactivity can be expressed as a function of time with the following equation

$$C = Ae^{-\alpha t} + Be^{-\beta t}.$$

In vivo distribution

Thirty mice with the body weight range of 18–24 g were randomly divided into six groups and injected via the tail vein with each radioactive agent of 0.2 mL aqueous solution and approximately 7.4 MBq of radioactivity. The mice were sacrificed by decapitation at 5, 15, 30, 60, 120 and 240 min post injection. Interested organs were collected and weighed, and 200 μL of blood were taken from carotid artery. The radioactivity of each sample was measured using a γ counter. The distribution of the radioactivity in different organs was calculated and expressed as

$$\%\mathrm{ID/g} = \frac{\text{organ CPM}}{\text{organ weight} \times \text{injected CPM}} \times 100\ \%.$$

Results and discussion

Chemistry and radiolabeling

EIPrDP, EIBDP, and EIPeDP were synthesized in four steps from the starting material 2-ethylimidazole (Scheme 1). Nucleophilic substitution of the bromoestes generated the imidazole-substituted esters. Hydrolysis of the esters under acidic conditions gave the carboxylic acid **2a–c**. Nucleophilic addition of PCl_3 to carboxylic acids under strong acidic conditions generated α-hydroxy phosphoric chlorides, which hydrolyzed in water to give diphosphates **3a–c**. ^{99m}Tc-EIPrDP, ^{99m}Tc-EIBDP and ^{99m}Tc-EIPeDP were synthesized from the reaction of the diphosphates and $^{99m}TcO_4^-$ under reducing conditions (scheme 1). TLC analysis showed that $Na^{99m}TcO_4$ was completely reduced and ^{99m}Tc-colloidal amount was less than 2 % (results of **4a** is shown in Fig. 1). All three tracers showed similar results. HPLC analysis revealed that free technetium ($Na^{99m}TcO_4$) eluted at 8.9 min, while **4a–4c** eluted at 2.8 ± 0.1 min (Fig. 2). The nearly identical retention times of **4a–c** indicated the structural analogy of these ^{99m}Tc-DPs [17]. Furthermore, the single peak in the HPLC-chromatogram clearly shows one complex, no residual $Na^{99m}TcO_4$, or other ^{99m}Tc impurities [28]. This labeling method meets clinical requirements for production of other ^{99m}Tc-labeled diphosphonates, such as ^{99m}Tc-MDP. These radiolabeled compounds were used immediately for both in vitro and in vivo studies.

In vitro stability

More than 95 % of ^{99m}Tc-EIPrDP, ^{99m}Tc-EIBDP and ^{99m}Tc-EIPeDP remained intact in the PBS, FBS and HS after 6 h of incubation (Fig. 3). The results indicated that these complexes are stable enough for biodistribution and imaging studies.

Log *P* value and plasma protein binding

The octanol–water partition coefficient (log *P*) for ^{99m}Tc-EIPrDP, ^{99m}Tc-EIBDP and ^{99m}Tc-EIPeDP were −1.70,

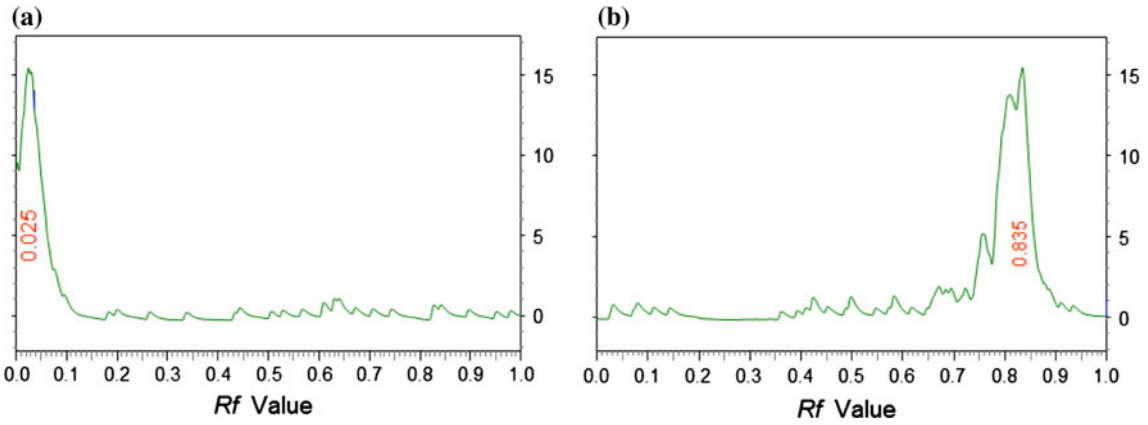

Fig. 1 TLC analyses of **4a**: **a** developed in acetone (R_f values for $^{99m}TcO_2{\cdot}nH_2O$ and **4a** were 0–0.1, for $Na^{99m}TcO_4$, 0.9–1); **b** developed in H_2O (R_f value for $^{99m}TcO_2{\cdot}nH_2O$ was 0–0.1, for **4a** was 0.8–0.9, for $Na^{99m}TcO_4$ was 0.9–1)

−1.67, −1.65 in PBS at pH = 7.4 (Table 1). The lipophilicity of these complexes increases with the length of the carbon chain between the imidazolyl and geminal diphosphonates group. The log *P* values are important parameters for the biological distribution of these complexes [31].

The percentages of plasma protein binding for ^{99m}Tc-EIPrDP, ^{99m}Tc-EIBDP, and ^{99m}Tc-EIPeDP, were 23.12, 22.74, and 23.24, respectively (Table 1). In general, the binding has significant influence on the bone uptake in the biodistribution [32]. However, almost no change in plasma protein binding was observed for this series of complexes, although the length of the carbon chain increased from 2 to 4. In contrast, the log *P* values and plasma protein binding observed here are larger than those for ^{99m}Tc-MIPrDP, ^{99m}Tc-MIBDP and ^{99m}Tc-MIPeDP [26], reflecting much stronger influence of substituents in the imidazole ring.

Kinetics of blood clearance

Pharmacokinetics of **4a–4c** can be fitted with double exponential equations, $C = 12.11e^{-0.110t} + 4.36e^{-0.016t}$, $C = 19.78e^{-0.101t} + 3.27e^{-0.013t}$ and $C = 17.38e^{-0.057t} + 0.794e^{-0.0046t}$, during 6 h post injection, respectively (Table 2; Fig. 4). The K_{12} and K_{21} of ^{99m}Tc-EIPeDP were 0.043 and 0.041 min^{-1} respectively, which were higher than those of ^{99m}Tc-EIBDP or ^{99m}Tc-EIPeDP. The values of CL were 0.95, 0.856 and 0.782 %ID/g min^{-1} and the AUC were 388, 432, 472 for ^{99m}Tc-EIPrDP, ^{99m}Tc-EIBDP and ^{99m}Tc-EIPeDP, respectively. The blood clearance of ^{99m}Tc-EIPrDP was faster than that of ^{99m}Tc-EIBDP or ^{99m}Tc-EIPeDP in the early times.

Biodistribution studies

The complexes **4a–4c** mainly accumulated in the bone, kidneys, and liver (Table 3). The uptake of **4a–4c** in bone

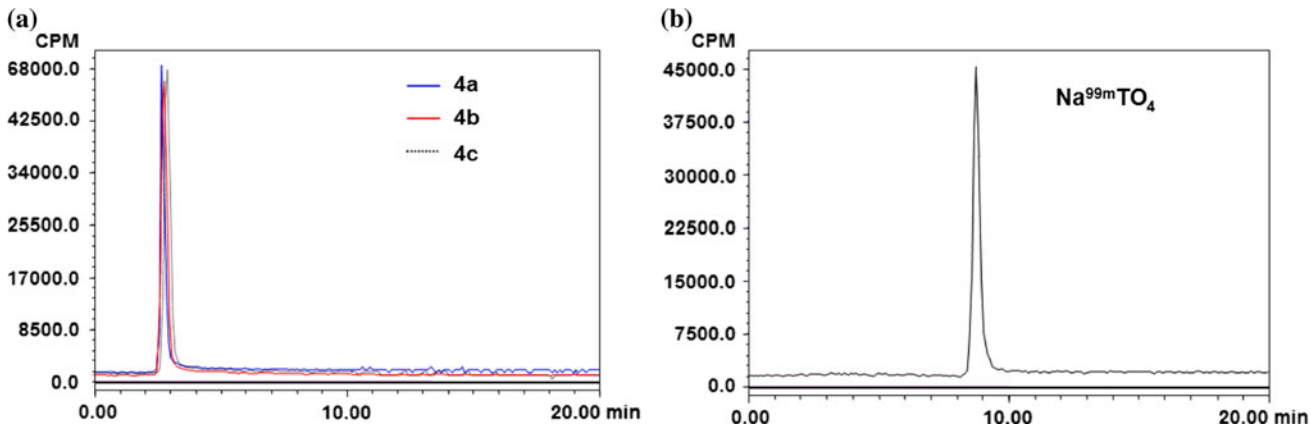

Fig. 2 HPLC analyses: **a** **4a** rt = 2.75 min, **4b** rt = 2.79 min, **4c** rt = 2.85 min; **b** $^{99m}TcO4^-$ rt = 8.95 min)

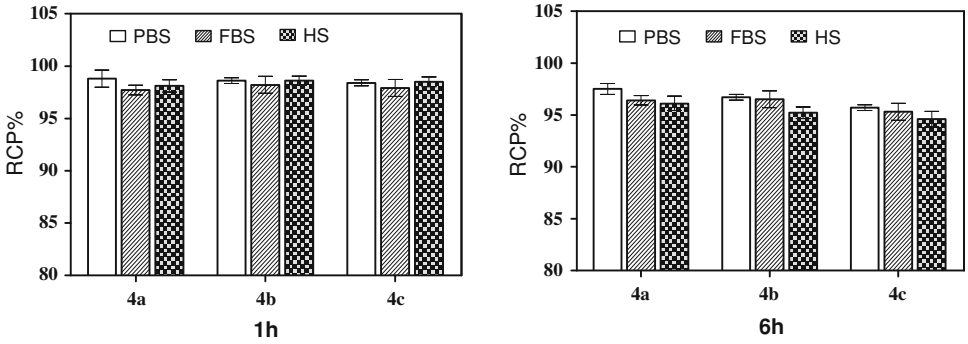

Fig. 3 In vitro stability of **4a–4c** in PBS, FBS, and human serum after incubation at 1 h and 6 h at 37 °C,respectively. Data were expressed as the mean ± SD

Table 1 Values of octanol–water partition coefficient and plasma protein binding

Constituent	Octanol–water partition coefficient	Plasma protein binding %
^{99m}Tc-EIPrDP	−1.70 ± 0.06	23.12 ± 0.49
^{99m}Tc-EIBDP	−1.67 ± 0.08	22.74 ± 0.81
^{99m}Tc-EIPeDP	−1.65 ± 0.11	23.24 ± 0.59

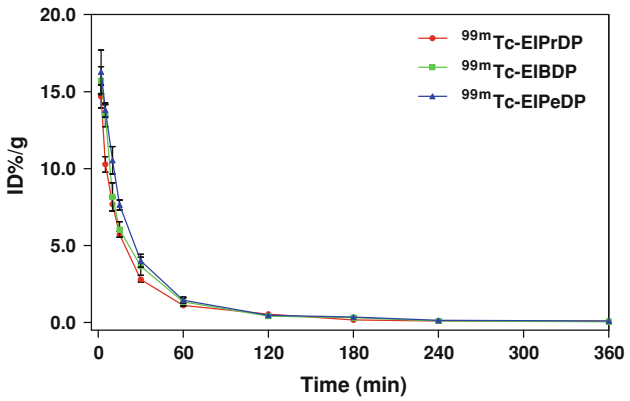

Fig. 4 Pharmacokinetic curves of ^{99m}Tc-EIPrDP, ^{99m}Tc-EIBDP and ^{99m}Tc-EIPeDP in mice ($n = 5$, mean ± SD)

peaks from 60 min to 120 min post injection at 13.3 ± 1.23, 11.7 ± 0.28 and 8.69 ± 0.04 %ID/g for ^{99m}Tc-EIPrDP, ^{99m}Tc-EIBDP and ^{99m}Tc-EIPeDP, respectively. From previous work of our group, we found that the bone uptake increases along with the increase of carbon chain between the imidazolyl and geminal diphosphonate groups in ZL (from ^{99m}Tc-ZL to ^{99m}Tc-IPeDP) [25, 27]. The same trend was observed for ^{99m}Tc-labeled methyl-substituted DPs (from ^{99m}Tc-MIPrDP to ^{99m}Tc-MIPeDP) [26]. At constant carbon chain length, the bone uptake increases along with size of the alkyl substituents in the imidazole ring. The bone uptake at 5 and 60 min for ^{99m}Tc-IPrDP [25], ^{99m}Tc-MIPrDP [26], and ^{99m}Tc-EIPrDP (Table 3), were 3.19 and 4.69, 6.43 and 12.2, and 8.63 and 13.3 %ID/g, respectively. Here the trend of bone uptake has reversed, with ^{99m}Tc-EIPeDP at lowest, indicating that optimal number of the carbon chain exists for bone uptake of the radiotracers, with ^{99m}Tc-EIPrDP as the best so far.

Table 2 Pharmacokinetic parameters of **4a–4c** in mice

Parameters	^{99m}Tc-EIPrDP, **4a**	^{99m}Tc-EIBDP, **4b**	^{99m}Tc-EIPeDP, **4c**
$K_{12}(min^{-1})$	0.043	0.035	0.017
$K_{21}(min^{-1})$	0.041	0.026	0.0069
K_e (min^{-1})	0.042	0.053	0.038
CL(%ID/g/min)	0.95	0.86	0.78
$T_{1/2\alpha}$ (min)	6.3	6.8	12.0
$T_{1/2\beta}$ (min)	44	50	149
AUC (%ID/g × min)	388	432	472

K_{12} rate constant of central compartment to peripheral compartment, K_{21} rate constant of peripheral compartment to central compartment, *Ke* elimination rate constant, *CL* total clearance rate, $T_{1/2\alpha}$ distribution half-life, $T_{1/2\beta}$ elimination half-life, *AUC* area under the C–T curve

No sign of toxicity through the study period was observed for **4a–4c**. This is consistent with the general observation that ZL has low toxicity and can be used therapeutically at a high dose [33, 34].

4a–4c also showed predominant kidney and liver uptake (Table 3). After 2 h post injection, the kidneys uptakes of **4a–4c** were 2.89 ± 0.11, 6.24 ± 0.23 and 3.25 ± 0.44 %ID/g, respectively; and the liver uptakes were 0.81 ± 0.02, 0.49 ± 0.03 and 1.50 ± 0.06 %ID/g, respectively. ^{99m}Tc-EIPeDP showed the highest liver uptake, suggesting that it not only cleared through the kidneys, but also was excreted by the liver. This kind of metabolic pathway increases the burden of liver.

Furthermore, **4a–4c** cleared from the blood rapidly, with 5.59 ± 0.31, 5.15 ± 0.27 and 8.51 ± 0.17 % ID/g at 5 min post injection, and 0.10 ± 0.01, 0.25 ± 0.01 and

Table 3 Biodistribution of **4a–4c** in mice (mean ± SD, $n = 5$)

Tissue	Time after injection					
	5 min	15 min	30 min	60 min	120 min	240 min
^{99m}Tc-EIPrDP, **4a**						
Heart	1.87 ± 0.03	0.72 ± 0.02	0.29 ± 0.01	0.15 ± 0.02	0.12 ± 0.00	0.08 ± 0.00
Liver	1.25 ± 0.23	1.35 ± 0.08	1.11 ± 0.09	0.99 ± 0.03	0.81 ± 0.02	0.97 ± 0.05
Spleen	0.74 ± 0.03	0.33 ± 0.02	0.22 ± 0.01	0.14 ± 0.01	0.09 ± 0.00	0.07 ± 0.01
Kidney	7.69 ± 0.11	4.82 ± 0.04	3.88 ± 0.01	3.53 ± 0.24	2.89 ± 0.11	2.65 ± 0.27
Muscle	1.23 ± 0.01	0.57 ± 0.01	0.25 ± 0.03	0.12 ± 0.01	0.07 ± 0.00	0.05 ± 0.01
Blood	5.59 ± 0.31	2.16 ± 0.09	0.86 ± 0.04	0.35 ± 0.00	0.10 ± 0.01	0.05 ± 0.00
All bone	8.63 ± 0.06	9.42 ± 0.67	12.7 ± 0.51	13.3 ± 1.23	11.6 ± 0.27	11.2 ± 1.74
^{99m}Tc-EIBDP, **4b**						
Heart	1.42 ± 0.15	0.68 ± 0.052	0.41 ± 0.01	0.24 ± 0.01	0.17 ± 0.01	0.08 ± 0.04
Liver	1.17 ± 0.14	0.95 ± 0.036	0.68 ± 0.02	0.53 ± 0.04	0.49 ± 0.03	0.26 ± 0.04
Spleen	0.86 ± 0.04	0.54 ± 0.015	0.34 ± 0.02	0.25 ± 0.03	0.17 ± 0.01	0.09 ± 0.01
Kidney	13.3 ± 0.54	6.83 ± 0.512	6.90 ± 3.04	5.96 ± 0.13	6.24 ± 0.23	5.26 ± 0.27
Muscle	1.42 ± 0.02	0.52 ± 0.010	0.33 ± 0.01	0.20 ± 0.01	0.13 ± 0.02	0.05 ± 0.00
Blood	5.15 ± 0.27	2.36 ± 0.200	1.32 ± 0.08	0.53 ± 0.04	0.25 ± 0.01	0.10 ± 0.01
All bone	7.58 ± 0.38	9.18 ± 0.480	11.6 ± 0.17	11.7 ± 0.28	10.6 ± 0.10	9.37 ± 0.34
^{99m}Tc-EIPeDP, **4c**						
Heart	3.35 ± 0.52	1.25 ± 0.08	0.55 ± 0.04	0.27 ± 0.01	0.18 ± 0.02	0.17 ± 0.02
Liver	1.57 ± 0.01	1.51 ± 0.11	1.55 ± 0.05	1.62 ± 0.09	1.50 ± 0.06	1.52 ± 0.02
Spleen	10.3 ± 0.93	0.70 ± 0.06	0.55 ± 0.08	0.36 ± 0.02	0.24 ± 0.02	0.29 ± 0.06
Kidney	0.18 ± 0.03	2.94 ± 0.53	6.60 ± 0.11	4.43 ± 0.45	3.25 ± 0.44	4.52 ± 0.03
Muscle	2.20 ± 0.44	0.61 ± 0.04	0.40 ± 0.04	0.23 ± 0.02	0.12 ± 0.01	0.10 ± 0.01
Blood	8.51 ± 0.17	4.07 ± 0.25	1.71 ± 0.29	0.63 ± 0.06	0.26 ± 0.01	0.10 ± 0.02
All bone	6.47 ± 0.24	7.24 ± 0.47	8.04 ± 0.80	8.69 ± 0.04	10.1 ± 0.55	8.73 ± 0.42

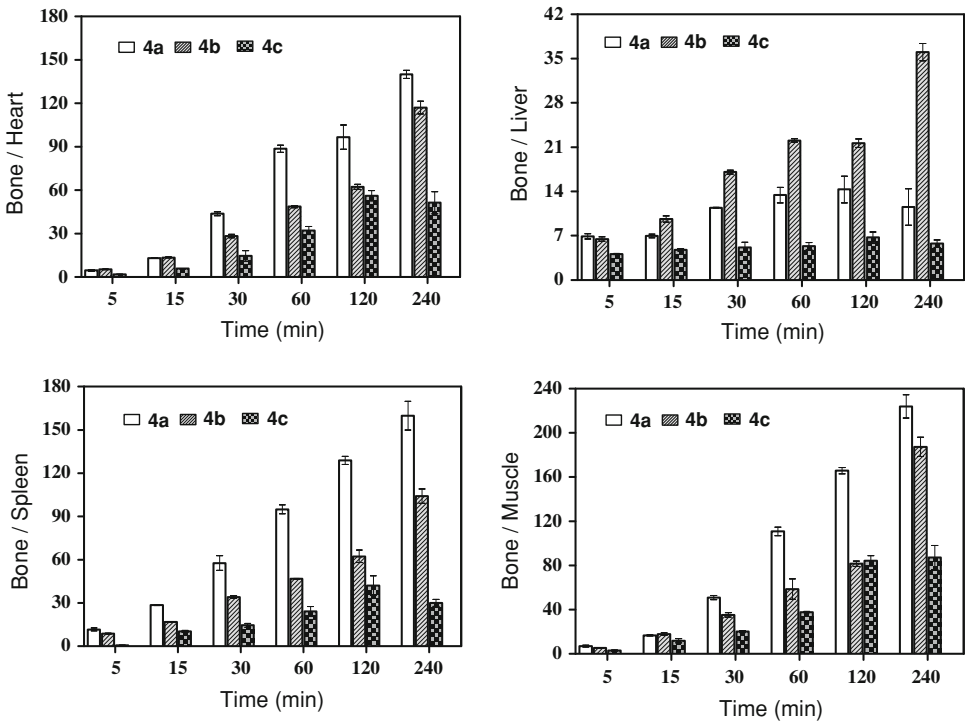

Fig. 5 Uptake ratios of bone to soft tissues in mice at different time post injection of **4a–4c**

0.26 ± 0.01 %ID/g 2 h post injection (Table 3). ^{99m}Tc-EIPeDP has higher radioactivity level than ^{99m}Tc-EIPrDP or ^{99m}Tc-EIBDP. This is consistent with the previous observation that ^{99m}Tc-EIPeDP excreted more from liver than ^{99m}Tc-EIPrDP or ^{99m}Tc-EIBDP does.

The uptake ratios of bone to muscle, spleen and heart for ^{99m}Tc-EIPrDP were larger than those of ^{99m}Tc-EIBDP and ^{99m}Tc-EIPeDP, while the ratio of bone to liver is the best for ^{99m}Tc-EIBDP (Fig. 5). The results showed that ^{99m}Tc-EIPrDP had higher selective uptake in the skeletal system and lower background uptake in soft tissues, and held great potential as a better bone-imaging agent among these ^{99m}Tc-DPs. No advantage was observed for elongating the carbon chain between the ethyl-imidazolyl and geminal diphosphonate groups. ^{99m}Tc-EIPrDP is worthy of further investigation.

The uptake ratios of bone-to-soft tissue for ^{99m}Tc-EIPrDP are the best, compared with other ^{99m}Tc-DPs previously evaluated in our lab. At 60 min post injection of ^{99m}Tc-EIPrDP, the ratios of bone to muscle, liver, spleen were 111, 13, 95, respectively, while those for ^{99m}Tc-IPrDP and ^{99m}Tc-MIPrDP were 18, 0.14, 0.46 and 64, 13, 29, respectively [25–27].

The bone uptake of ^{99m}Tc-EIPrDP peaks the earliest at 60 min among ^{99m}Tc-IPrDP [25, 27], ^{99m}Tc-MIPrDP [26], ^{99m}Tc-EIBDP and ^{99m}Tc-EIPeDP. In the clinical applications, shorter interval between injection and bone imaging would reduce the total examination time for patients.

Conclusions

A series of novel complexes of technetium-99m and ethyl-substituted zoledronic acids (^{99m}Tc-EIPrDP, ^{99m}Tc-EIBDP and ^{99m}Tc-EIPeDP) were prepared, with high radiolabeling yield and radiochemical purity (96 ± 2 %). They were stable up to 6 h in PBS, FBS and HS. The biodistribution in mice showed that ^{99m}Tc-EIPrDP was best among the complexes examined. Moreover, ^{99m}Tc-EIPrDP shows higher bone accumulation in the skeletal system and lower background in soft tissues at 60 min, as compared with ^{99m}Tc-IPrDP and ^{99m}Tc-MIPrDP. We will continue to explore ^{99m}Tc-EIPrDP as a SPECT imaging agent in larger animals and animal models of bone metastases.

Acknowledgments The authors are very grateful to the National Natural Science Foundation of China (20801024 and 21001015), Natural Science Foundation of Jiangsu Province (BK2009077), and Key Medical Talent Project of Jiangsu Province (RC2011097) for their financial support.

References

1. Costa L, Major PP (2009) Nat Clin Pract Oncol 6:163–174
2. Selvaggi G, Scagliotti GV (2005) Crit Rev Oncol Hematol 56:365–378
3. Palma E, Correia JD, Campello MP, Santos I (2011) Mol Biosyst 7:2950–2966
4. Motaleb MA, Sakr TM (2011) J Label Compd Radiopharm 54:597–601
5. Valdez VA, Jacobstein JG (1980) J Nucl Med 21:47–49
6. King MA, Weber DA, Casarett GW, Burgener FA, Corriveau O (1980) J Nucl Med 21:22–30
7. Davis MA, Jones AG (1976) J Nucl Med 6:19–31
8. Subramanian G, McAfee JG, Blair RJ, Kallfelz FA, Thomas FD (1975) J Nucl Med 16:744–755
9. Fogelman I, Pearson DW, Bessent RG, Tofe AJ, Francis MD (1981) J Nucl Med 22:880–883
10. Cole TJ, Balseiro J, Lippman HR (1991) J Nucl Med 32:325–327
11. Shalaby RE, Majd M (2001) J Nucl Med 42:878–883
12. Fleisch H, Graham R, Russell G, Francis MD (1969) Science 19:1262–1264
13. Vasireddy S, Talwarkar A, Miller H (2003) Clin Rheumatol 22:376–380
14. Robert EC, Eugene VM (2011) Bone 49:71–76
15. Love C, Din AS, Tomas MB, Kalapparambath TP, Palestro CJ (2003) Radiographics 23:341–358
16. Ogawa K, Mukai T, Inoue Y, Ono M, Saji H (2006) J Nucl Med 47:2042–2047
17. Kanis JA, Gertz BJ, Singer F, Ortolani S (1995) Osteoporos Int 5:1–13
18. Frank HE, Anne ML, Hogan SS, Maria KT, Xuchen D, James TT, Aaron AK, James ED, Bobby LB, Udo O, Mark WL, Alan B, Boris AK, Charles EM (2011) Bone 49:20–33
19. Smith MR (2008) Urol Oncol Semin Orig Investig 26:420–425
20. Luo SN, Wang HY, Xie MH (2005) Chin J Nucl Med 6:342–343
21. Niu GS, Luo SN, Yan XH, Yang M, Ye WZ, Wang HY (2008) Nucl Tech (in Chinese) 31:698–701
22. Chen CQ, Luo SN, Lin JG, Yang M, Ye WZ, Qiu L (2009) Nucl Sci Tech 20:302–306
23. Lin JG, Luo SN, Chen CQ, Qiu L, Wang Y, Cheng W (2010) Appl Radiat Isot 9:1616–1622
24. Wang Y, Luo SN, Lin JG, Qiu L, Cheng W, Zhai HZ, Nan BB, Ye WZ, Xia YM (2011) Appl Radiat Isot 69:1169–1175
25. Lin JG, Qiu L, Cheng W, Luo SN, Ye WZ (2011) Nucl Med Biol 38:619–629
26. Qiu L, Cheng W, Lin JG, Luo SN, Xue L (2011) Molecules 16:6165–6178
27. Lin JG, Qiu L, Cheng W, Luo SN, Xue L, Zhang S (2012) Appl Radiat Isot 70:848–855
28. Verbeke K, Rozenski J, Cleynhens B, Vanbilloen H, Groot T, Weyns N, Bormans G, Verbruggen A (2002) Bioconjug Chem 13:16–22
29. Widler L, Jaeggi KA, Glatt M, Müller K, Bachmann R, Bisping M, Born AR, Cortesi R, Guiglia G, Jeker H (2002) J Med Chem 45:3721–3738
30. Prata MIM, Santos AC, Bligh SWA, Chowdhury AHMS (2000) Nucl Med Biol 27:605–610
31. Valko KJ (2004) J Chromatogr A 1037:299–310
32. Kroesbergen J, Roozen AMP, Wortelboer MR, Gelsema WJ, DeLigny CL (1988) Nucl Med Biol 5:479–487
33. Major P, Lortholary A, Hon J, Abdi E, Mills G, Menssen HD, Yunus F, Bell R (2001) J Clin Oncol 19:558–567
34. Berenson JR (2005) Oncologist 10:52–62